Heterotypic interactions in the dilute phase can drive co-condensation of prion-like low-complexity domains of FET proteins and mammalian SWI/SNF complex

Authors: Richoo B. Davis[1], Aishwarya Kanchi Ranganath[2], Mahdi Muhammad Moosa[1], Priya R. Banerjee[1, 2, *]

Affiliations:
[1]Department of Physics, University at Buffalo, Buffalo NY 14260, USA
[2]Department of Chemical and Biological Engineering, University at Buffalo, Buffalo NY 14260, USA

*Corresponding author: prbanerj@buffalo.edu

Abstract

Prion-like domains (PLDs) are low-complexity protein sequences enriched within nucleic acid-binding proteins including those involved in transcription and RNA processing. PLDs of FUS and EWSR1 play key roles in recruiting chromatin remodeler mammalian SWI/SNF complex to oncogenic FET fusion protein condensates. Here, we show that disordered low-complexity domains of multiple SWI/SNF subunits are prion-like with a strong propensity to undergo intracellular phase separation. These PLDs engage in sequence-specific heterotypic interactions with the PLD of FUS in the dilute phase at sub-saturation conditions, leading to the formation of PLD co-condensates. In the dense phase, homotypic and heterotypic PLD interactions are highly cooperative, resulting in the co-mixing of individual PLD phases and forming spatially homogeneous ternary co-condensates. Heterotypic PLD-mediated positive cooperativity in protein-protein interaction networks is likely to play key roles in the assembly of SWI/SNF complexes and their co-phase separation with transcription factors containing homologous low-complexity domains.

Introduction

Biomolecular condensates such as stress granules and transcription factories are membrane-less subcellular bodies that form and are regulated via the phase separation of multivalent proteins and nucleic acids [1–3]. The perceived physiological functions of biomolecular condensates range from signaling hubs under normal conditions to storage depots in response to cellular stress [3]. Sequence analyses of the proteins enriched in intracellular condensates both in the nucleus and cytoplasm have previously revealed an abundance of proteins containing long stretches of intrinsically disordered prion-like domains [4,5]. Prion-like domains (PLDs) are typically characterized by their low complexity sequence features with an overrepresentation of aromatic (Y/F) and polar amino acids (G/S/Q/N) and depletion of charged residues [6,7]. Proteins with PLDs have been identified in all life forms [8–12]. Prion proteins were initially discovered as proteinaceous infectious agents in bovine spongiform encephalopathy and other neurodegenerative diseases [4,13–15], but are increasingly recognized with key functional roles in driving phase separation of RNA-binding proteins in the cell, and in the formation of functional amyloids [16,17].

What roles do PLDs play in the context of protein phase separation? Multivalent interactions between PLDs and with the solvent, which are encoded by the PLD sequence composition and patterning [18,19], have been recognized to be a key feature driving the phase separation of isolated PLD chains and PLD-containing proteins [20–25]. Previous studies using hnRNP A1 PLD have demonstrated that the distributed aromatic (Y/F) amino acids act as “stickers” that mediate PLD-PLD interactions [18,26], whereas the polar amino acids (Q/S/G) can be described as “spacers”, which regulate chain solvation and cooperativity of sticker-sticker interactions. Together, the sticker and spacer residues regulate PLD phase separation in a context-dependent manner [19]. When part of a multi-domain protein, π-π and cation-π interactions mediated by the aromatic sticker residues of PLDs have been shown to encode the driving force for phase separation of many RNA and DNA binding proteins including FUS, EWSR1, TAF15, hnRNP A1, and EBF1 [21,27–29]. Further, debilitating point mutations in PLDs have been reported to promote the pathological transformation of protein condensates from a liquid-like state to solid aggregates [20,30,31]. Thus, PLDs play important roles in the context of functional protein phase separation as well as disease processes associated with the formation of aberrant biomolecular condensates.

Many intracellular biomolecular condensates, such as stress granules and transcriptional hubs, are known to contain a multitude of proteins containing prion-like low complexity domains [4,5,32]. Despite being broadly classified as prion-like based on the frequencies of certain amino acids in a protein sequence [6,7], individual PLD chains typically feature distinct sequence composition, amino acid patterning, and chain length [4,22,33]. Do PLDs from distinct proteins interact with one another and influence the phase separation of each other? Previous studies have reported that the PLDs in transcription factors, including the FET family of fusion oncoproteins, not only drive their phase separation but also facilitate the recruitment of essential coactivators, such as the catalytic subunit of the mammalian SWI/SNF complex, BRG1, in transcriptional condensates [28,34–37]. Interestingly, BRG1 contains an N-terminal PLD, which can engage with the PLD of FET fusion proteins via heterotypic multivalent interactions [28]. Although homotypic phase separation of some PLDs, such as FUS and hnRNP A1, are well characterized [18,19,27], little is

known about how heterotypic interactions regulate the co-phase separation of PLD mixtures. In multi-component mixtures, multivalent homotypic and heterotypic interactions between PLD chains can either positively or negatively cooperate, resulting in a rich phase behavior and dense phase co-partitioning. Further, PLD-containing proteins such as FUS have recently been reported to form a heterogeneous pool of oligomeric complexes below their saturation concentration for phase separation [38], which are thought to represent distinct functional states of the protein than the condensates that form at higher concentrations [39]. However, a key unanswered question is whether heterotypic PLD interactions occur at sub-saturation conditions, which may provide a mechanistic basis for the formation of functional protein complexes, such as the FET proteins and BRG1, driving oncogenic transcriptional programs.

Motivated by these open questions, here we systematically investigate the phase behavior of PLD mixtures encompassing FUS^{PLD} and the PLDs from the chromatin remodeler mammalian SWI/SNF (mSWI/SNF) complex that aberrantly interact with FUS fusion oncoproteins in transcriptional reprogramming [40]. Our study incorporates newly discovered PLDs from four mSWI/SNF complex subunits: ARID1A, ARID1B, SS18, and BRG1, which are essential components for spatiotemporal transcriptional regulation and chromatin remodeling [41–43]. Employing in vitro experiments with reconstituted PLD systems in conjunction with cell culture models, we show that there exists a broad range of saturation concentrations (C_{sat}) of PLD chains in vitro that directly correlate with their ability to form phase-separated condensates in live cells. Surprisingly, we find that except BRG1, mSWI/SNF subunit PLDs undergo phase separation with C_{sat} values substantially lower than the previously reported PLDs of RNA binding proteins, including FUS^{PLD} [18,27]. This enhanced propensity of mSWI/SNF subunit PLD phase separation is due to their longer chain length as compared to the PLD of FUS. We further show that in ternary mixtures, mSWI/SNF subunit PLDs significantly lower the saturation concentration for phase separation of FUS^{PLD}. Quantitative confocal fluorescence microscopy revealed that heterotypic PLD interactions result in their co-partitioning in the dense phase with partition coefficients that show a positive correlation with the number of aromatic and arginine stickers. Interestingly, we find that heterotypic PLD-PLD interactions between FUS and mSWI/SNF subunit occur at sub-saturation concentrations in vitro and in live cells, indicating strong affinities between these low complexity domains. Heterotypic PLD interactions in the dilute phase drive their co-phase separation. In ternary mixtures of PLD condensates, individual PLD dense phases undergo complete mixing, and together, they form spatially homogeneous PLD co-condensates. This finding indicates that homotypic and heterotypic PLD-PLD interactions are highly cooperative and thermodynamically compatible in the dense phase despite substantially different saturation concentrations of individual PLD chains. We conjecture that PLD-mediated interactions in the sub-saturation conditions between multiple subunits of the mSWI/SNF chromatin remodeling complex and FET proteins as well as their co-condensation may constitute an important step in establishing transcriptionally relevant protein interaction networks.

Results

Prion-like domains of mSWI/SNF subunits form dynamic phase-separated condensates in live cells

mSWI/SNF chromatin remodeler complex is enriched in subunits that have large disordered low complexity regions with unknown functions [44]. Many of these disordered regions have prion-like sequences (**Fig. S1**) [28]. Since PLDs of RNA and DNA binding proteins can drive phase separation and contribute to the formation of biomolecular condensates in cells [4,21,27], we investigated whether mSWI/SNF subunit PLDs are phase separation competent. We selected the top four PLDs in the complex based on their length, functional and disease relevance, which correspond to the following subunits - BRG1 [catalytic subunit], ARID1A, and ARID1B [among most mutated proteins in cancer [43]], and SS18 [relevant to fusion oncoprotein SS18-SSX [45]] (**Fig. 1a&b**; **Fig. S1**). We noted that although the prion prediction algorithm PLAAC [6] categorizes these low complexity domains as prion-like, these PLDs have varying sequence composition and their lengths are significantly higher than the PLDs from RNA binding proteins (**Fig. 1b**; **Tables S1-3**). To determine if they were phase separation competent, we titrated concentrations of recombinant PLDs in vitro (buffer: 125mM NaCl, 25mM Tris.HCl pH 7.5) and observed that apart from BRG1^{PLD}, all other PLDs form spherical condensates in a concentration-dependent manner (**Fig. 1c; Fig. S2a**). Further, ARID1B^{PLD} condensates showed cluster-like morphologies upon phase separation, suggesting a percolation-type network formation [46] (**Fig. 1c**). Based on the optical microscopy data, we quantified the saturation concentrations (C_{sat}) for the PLDs as $\leq$ 2.5 μM for ARID1A^{PLD} and SS18^{PLD}, and $\leq$ 5 μM for ARID1B^{PLD} (**Fig. 1d**; **Fig. S2a**). Under similar experimental conditions, FUS^{PLD} undergoes phase separation with a C_{sat} of $\leq$ 200 μM (**Fig. S2a**) [47], which is almost two orders of magnitude higher than ARID1A^{PLD} and SS18^{PLD}. Although BRG1^{PLD} did not phase separate under these conditions (**Fig. S2a**) it can be induced to form spherical condensates in presence of a macromolecular crowder (20% Ficoll PM70; **Fig. S2b**) [28]. These data suggest that except for BRG1, mSWI/SNF subunit PLDs are highly phase separation competent. We next probed whether these condensates are dynamic using fluorescence recovery after photobleaching (FRAP) experiments. FRAP recovery traces indicate that all PLD condensates rapidly exchange molecules (**Fig. 1e**). Based on the FRAP traces, we find that ARID1A^{PLD} forms the most dynamic condensates with more than 80% recovery, SS18^{PLD} is intermediate with ~60% recovery and ARID1B^{PLD} is the least dynamic with less than 40% recovery within the same observational timeframe. The reduced dynamicity of ARID1B^{PLD} condensates is consistent with the percolation-driven network formation observed for these condensates (**Fig. 1c**).

Although PLDs have emerged as a driver of ribonucleoprotein phase separation under physiological and pathological conditions, expression of these domains alone typically does not lead to the formation of condensates in live cells [20,28,48,49]. This is consistent with their known C_{sat} values in vitro, which range from 100-200 μM and are typically much higher than their intracellular concentrations [18,27,47,50]. Since mSWI/SNF PLDs show low micromolar C_{sat} values in vitro, we posited that they may form condensates in live cells at low expression levels. To test this idea, we transiently transfected HEK293T cells with GFP-PLD plasmids. Upon expression, ARID1A^{PLD}, ARID1B^{PLD}, and SS18^{PLD} readily formed spherical nuclear foci, whereas BRG1^{PLD} and FUS^{PLD}

remained diffused at all expression levels (**Fig. 1f**). To estimate the relative C_{sat} of mSWI/SNF PLDs within the nucleus, we used GFP fluorescence intensity as a proxy for concentration and leveraged the stochastic nature of intracellular PLD expression. We observed that SS18$^{\mathrm{PLD}}$ has the lowest C_{sat} followed by ARID1A$^{\mathrm{PLD}}$ and ARID1B$^{\mathrm{PLD}}$ (**Fig. 1g**). This rank order of cellular saturation concentrations is similar to their in vitro phase behavior (**Fig. 1d**). Further, FRAP experiments revealed that the nuclear condensates of ARID1A$^{\mathrm{PLD}}$, ARID1B$^{\mathrm{PLD}}$, and SS18$^{\mathrm{PLD}}$ are highly dynamic (**Fig. 1h**). Interestingly, the morphology of the PLD condensates varied with their subcellular localization. Spherical condensates formed within the nucleus and irregular, yet dynamic, assemblies were observed in the cytoplasm (**Fig. S2c&d**). Such differences could arise from the distinct intracellular microenvironment of the cytoplasm and the nucleus, such as the viscoelasticity of chromatin fibers, altered post-translational modifications, and abundance of RNAs in the nucleus, which can markedly influence the coarsening behavior and biophysical properties of condensates [51–55].

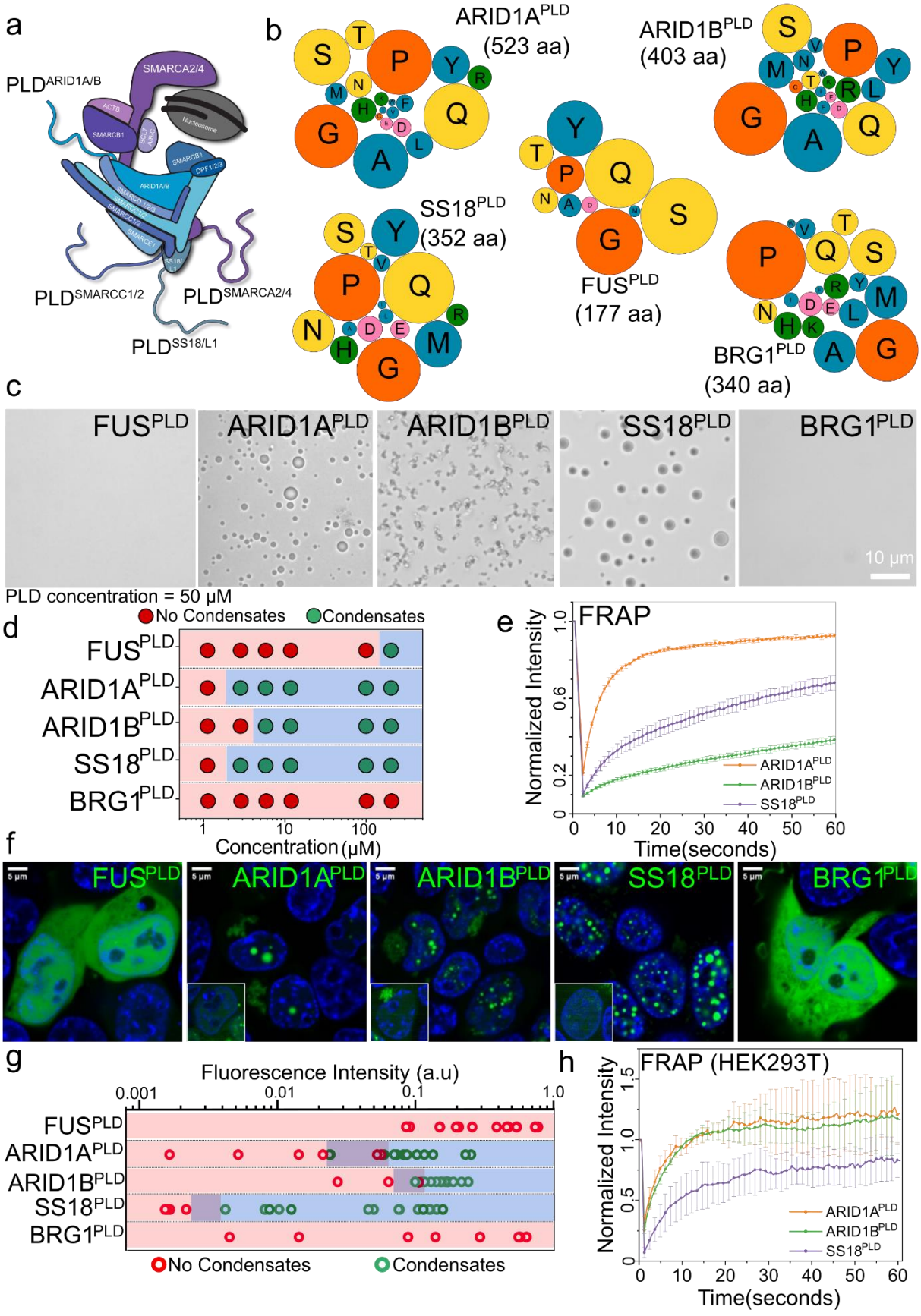

Figure 1: Prion-like domains of mSWI/SNF complex subunits form phase-separated condensates in vitro and in live cells. **a)** A schematic of the mSWI/SNF complex bound to the nucleosome. This is adapted from Varga et al., BST, 2021 [56]. The four largest prion-like domains (PLDs) in the mSWI/SNF complex are displayed as shaded lines**. b)** A bubble chart representation of the sequence composition of the five PLDs (FUS, ARID1A, ARID1B, SS18, and BRG1) used in this study. The lengths of the PLDs are displayed as amino acid count "aa". **c)** Differential interference contrast (DIC) microscopy images of purified FUS^{PLD} and mSWI/SNF PLDs at 50 μM protein concentration. **d)** Concentration titrations of various PLDs are displayed with green circles denoting the two-phase regime and red circles denoting the single-phase regime (*see* DIC images in **Fig. S2**). **e)** Fluorescence recovery after photobleaching (FRAP) curves for condensates formed by $ARID1A^{PLD}$, $ARID1B^{PLD}$, and $SS18^{PLD}$ at 50 μM concentrations. The FRAP curves show the average intensity and standard deviation of the intensity profiles over time (n ≥ 3). **f)** Fluorescence microscopy images of HEK293T cells expressing GFP-tagged PLDs (FUS^{PLD}, $ARID1A^{PLD}$, $ARID1B^{PLD}$, $SS18^{PLD}$ and $BRG1^{PLD}$), as indicated. Hoechst was used to stain the cell nucleus which is shown in blue. The insets show images of cells expressing GFP-tagged proteins below their respective saturation concentrations. **g)** The phase separation capacity is quantified over various levels of nuclear fluorescence intensity (a proxy for protein concentration). Green circles indicate the presence of nuclear condensates and red circles represent diffused expression patterns. The dark-shaded regions represent the transition concentrations. **h)** FRAP curves for condensates formed by GFP-tagged PLDs in HEK293T cells. The average intensity and standard deviation of the intensity profiles are shown over time (n = 3). The scale bar is 5 microns for all images.

The length of PLD chains determines their saturation concentration in live cells

The phase separation capacity of PLDs has been attributed to multivalent chain-chain interactions predominantly mediated by the distributed aromatic residues [18] and the chain-solvent interactions governed by polar residues such as Gly and Ser [19]. While $SS18^{PLD}$ has a lower percentage of aromatic content than FUS^{PLD} (**Tables S1-3**), it undergoes phase separation more robustly in vitro and in live cells as compared to FUS^{PLD} (**Fig. 1**; **Fig. S2**). We posited that this difference could arise from the chain length of the PLDs, given $SS18^{PLD}$ is approximately two-fold longer (352 aa) than FUS^{PLD} (173 aa). In general, increasing the chain length of a polymer can act as an entropic sink, thereby increasing the driving force for phase separation [48,57]. To test this idea, we designed a FUS^{PLD} variant where we doubled the length of PLD of FUS (346 aa), which we termed as FUS^{2XPLD} (**Fig. 2a**). In contrast to the FUS^{PLD} which remained diffused at all expression levels, we observed that FUS^{2XPLD} formed phase-separated condensates in the cell nucleus at a relatively low expression level (**Fig. 2b**), similar to the three mSWI/SNF subunit PLDs (**Fig. 1f**). The estimated intracellular saturation concentration of FUS^{2XPLD} was observed to be similar to that of $ARID1A^{PLD}$ and $ARID1B^{PLD}$ (**Figs. 2c & 1g**) and marginally higher than the $SS18^{PLD}$. Analogous to mSWI/SNF subunit PLD condensates, FRAP experiments revealed that FUS^{2XPLD} condensates have a high degree of dynamic behavior (**Fig. 2d**). These data collectively suggest that, in addition to their primary sequence features, PLD chain length is an important determinant of the driving force for PLD phase separation. However, we note that the chain length alone is not sufficient for driving the phase separation of PLDs. This is clearly highlighted by the weak phase separation propensity of $BRG1^{PLD}$ (**Fig. 1b-f**) which features almost the same length (340 aa) as the $SS18^{PLD}$ and FUS^{2XPLD}, but significantly reduced numbers of aromatic and arginine stickers (**Tables S1-3**).

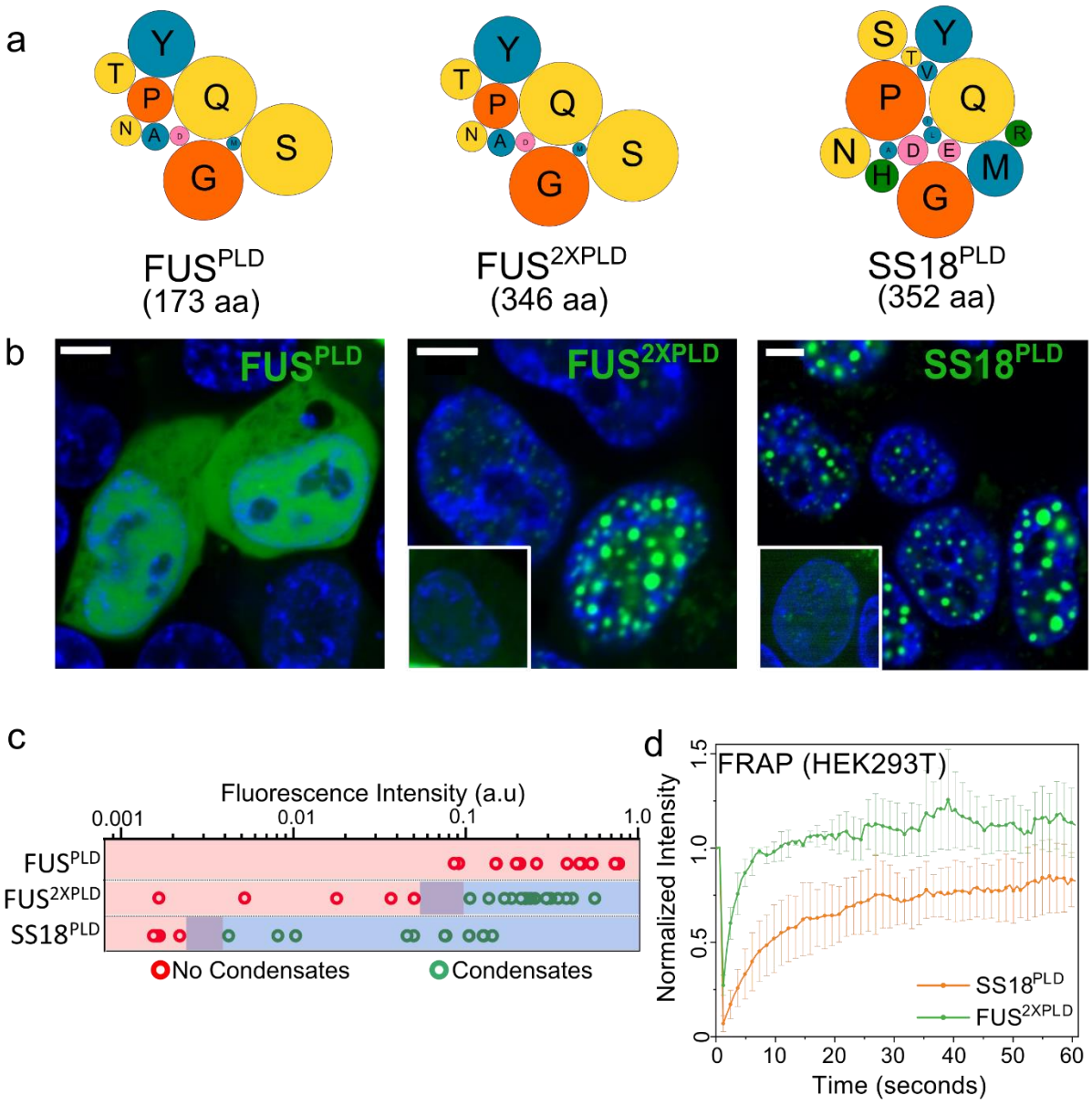

Figure 2: The length of the PLD chains influences their phase behavior inside cells. **a)** A bubble chart representation of the sequence composition of three PLDs. The lengths of the PLDs are displayed as amino acid count "aa". **b)** Fluorescence microscopy images of HEK293T cells expressing GFP-tagged proteins (FUS^{PLD}, FUS^{2XPLD}, or $SS18^{PLD}$), as indicated. Hoechst was used to stain the cell nucleus (shown in blue). The insets show images of cells expressing GFP-tagged proteins below their respective saturation concentration (diffused distribution). **c)** Phase separation capacities of PLDs are quantified over various levels of fluorescence intensity (a proxy for protein concentration). Green circles indicate the presence of condensates and red circles indicate an absence of condensates. The dark-shaded regions represent the transition concentrations. **d)** FRAP curve for condensates of GFP-tagged FUS^{2XPLD} and $SS18^{PLD}$ in HEK293T cells. The average intensity and standard deviation of the intensity profiles are shown over time (n = 3). The scale bar is 5 microns for all images.

mSWI/SNF PLD condensates recruit low-complexity domains of transcription factors and RNA polymerase II via heterotypic PLD-mediated interactions

An emerging feature underlying transcriptional regulation by prion-like low complexity domains in transcription factors is their ability to directly engage with chromatin remodeler SWI/SNF complexes [35,36,40] and RNA polymerase II (RNA pol II) [25], the C-terminal domain (CTD) of which also has a prion-like sequence (**Fig. S3**). Previous studies have reported that BRG1, the catalytic subunit of the mSWI/SNF complex, can enrich within optogenetically induced FUS^{PLD} condensates and FUS fusion protein condensates in live cells [28]. We posited that this functional engagement can be, in part, mediated by disordered PLDs of FUS and BRG1. Indeed, FUS^{2XPLD} condensates showed a strong colocalization with $BRG1^{PLD}$ in live cells (**Fig. S4**), which otherwise remains homogeneously distributed in the nucleus (**Fig. 1f**). This observation of $BRG1^{PLD}$ partitioning into FUS^{2XPLD} condensates clearly suggests the occurrence of heterotypic PLD-PLD interactions in these systems. To explore these heterotypic interactions systematically, we analyzed the degree of the partitioning of PLDs of FUS and RNA pol II into condensates formed by $ARID1A^{PLD}$, $ARID1B^{PLD,}$ and $SS18^{PLD}$. To this end, we defined scaffolds and clients in each pair of PLD mixtures: scaffold is the protein that forms condensates ($C > C_{\mathrm{sat}}$) and the client, defined as the protein that does not phase separate under the experimental conditions ($C < C_{\mathrm{sat}}$), partitions into the scaffold condensates (**Fig. 3a**). The degree of client partitioning is determined by the sequence-specific scaffold-client interactions and the chain solvation free energy difference between the dense phase and the dilute phase [58–60]. When the experimental conditions are the same and the scaffold concentration is fixed, partition coefficients, defined as $k = {I_{dense}}/{I_{dilute}}$, of a group of similar clients to a scaffold condensate can report on the relative strength of scaffold-client interactions [58,59]. In our experiments, we observe that each of the PLD condensates can recruit other PLDs (**Fig. 3b**), indicating a synergistic interplay between homotypic and heterotypic PLD interactions. However, the distribution of k values (**Fig. 3c**) spans over two orders of magnitude (~2−200), suggesting that there is a broad range of specificity of heterotypic interactions. We observed a few common trends for all three scaffold condensates: $SS18^{PLD}$, $ARID1A^{PLD}$, and $ARID1B^{PLD}$. Firstly, the partitioning of three strongly phase-separating mSWI/SNF PLDs within each other's condensates are similar and comparable to their self-partitioning (k ~ 50−220), suggesting that the homotypic PLD interactions are similar in strength as the heterotypic interactions between these PLDs. Secondly, $BRG1^{PLD}$, which showed a substantially low propensity of phase separation (weaker homotypic interactions) than the other PLDs, partitioning within mSWI/SNF PLD condensates is almost 15-100-fold lower (k ~ 2−5), suggesting substantially weaker heterotypic PLD interactions in this case. Interestingly, we observed that FUS^{PLD} partitioned in mSWI/SNF subunit PLD condensates to a similar degree as the $SS18^{PLD}$, $ARID1A^{PLD}$, and $ARID1B^{PLD}$, (k ~ 50−185) suggesting highly favorable heterotypic interactions. Finally, the CTD of RNA Pol II was observed to partition within mSWI/SNF PLD condensates to intermediate degrees (k ~ 20−80; **Fig. 3b&c**).

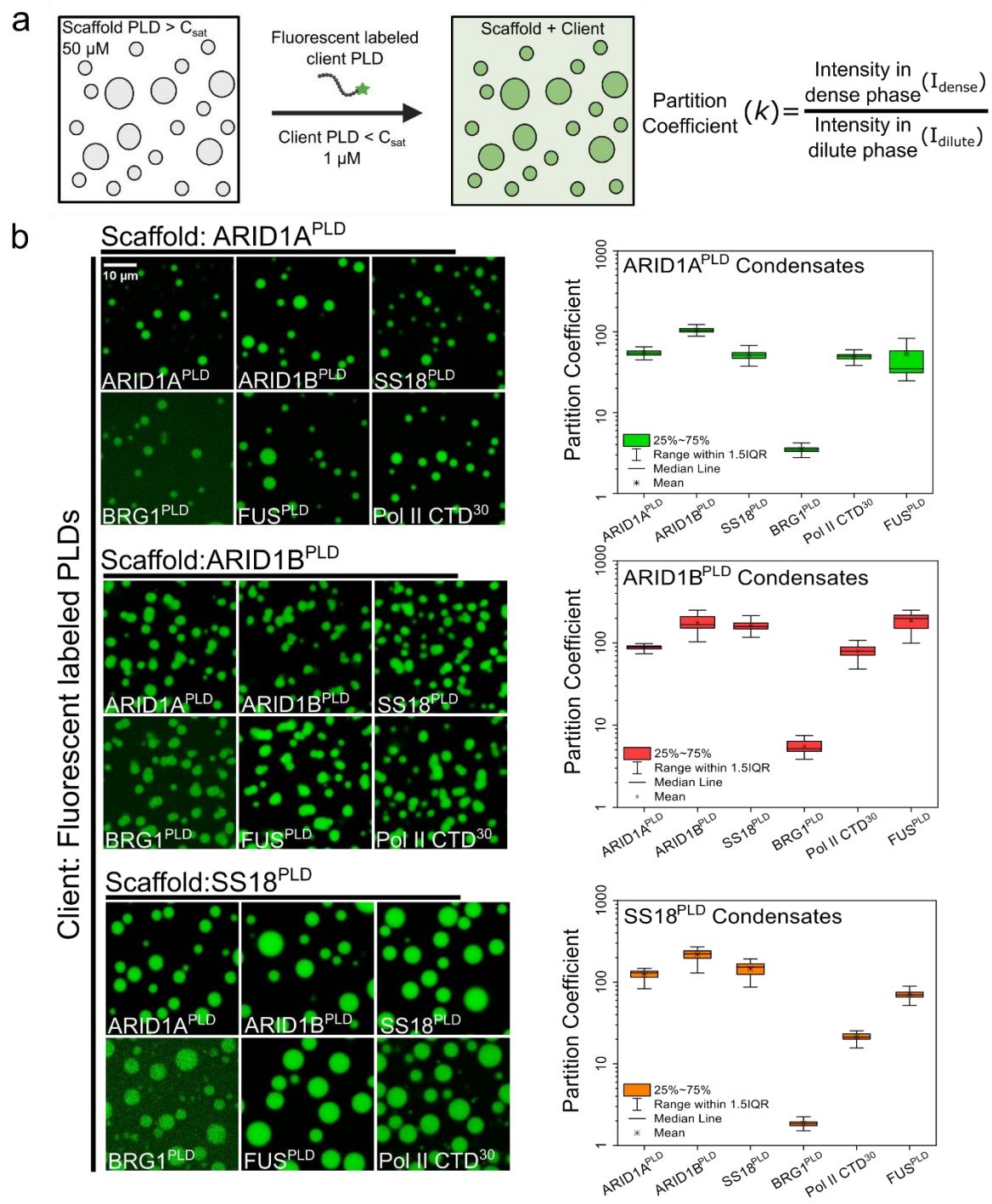

c

Partition coefficient of client (k)

Scaffold	ARID1A^{PLD} (523 aa)	ARID1B^{PLD} (403 aa)	SS18^{PLD} (352 aa)	BRG1^{PLD} (340 aa)	Pol II CTD^{30} (210 aa)	FUS^{PLD} (177 aa)
ARID1A^{PLD}	54.5 ± 4.1	104.5 ± 7.1	51.5 ± 6.6	3.5 ± .31	48.8 ± 4.7	53.3 ± 38.9
ARID1B^{PLD}	87.9 ± 5.5	177.3 ± 32.8	162.39 ± 20.2	5.5 ± .88	78.9 ± 13.3	185.4 ± 36.6
SS18^{PLD}	124.4 ± 15.6	218.3 ± 30.4	146.5 ± 27.7	1.8 ± .18	21.4 ± 2.1	71.5 ± 9.9

Figure 3: Heterotypic PLDs interact and enrich within homotypic PLD condensates. a) A Schematic of the co-partitioning assay based on confocal fluorescence microscopy. 50 μM concentration of the scaffold^{PLD} was used to form condensates and ~1 μM of the AlexaFluor488 labeled client^{PLD} was utilized to determine the partition coefficient (k). Created with BioRender.com. **b)** Partitioning of AlexaFluor488 labeled client PLDs (ARID1A^{PLD}, ARID1B^{PLD}, SS18^{PLD}, BRG1^{PLD}, RNA Polymerase II CTD[30], and FUS^{PLD}) within condensates of ARID1A^{PLD}, ARID1B^{PLD,} and SS18^{PLD}, respectively. Enrichment is calculated as shown in (**a**) and displayed as a box-and-whisker plot. **c)** The average partition coefficient (k) is tabulated along with the standard deviation from the mean. The scale bar is 10 microns.

Collective analysis of the experimental trend of partition coefficient data revealed a more positive correlation with the number of aromatic and arginine residues of the respective PLD chains (**Fig. S5**) than any other sequence features including the net charge per residues (NCPRs), number of hydrophobic residues, and PLD chain length. This observation indicates that the aromatic and arginine residues collectively act as stickers to drive homotypic phase separation of the system as well as heterotypic PLD-PLD interactions leading to their co-partitioning [18,19,27].

Heterotypic interactions drive PLD co-condensation in live cells

Based on the observed extent of heterotypic PLD interactions among mSWI/SNF subunit PLDs and with FUS^{PLD} in our in vitro client partitioning assay (**Fig. 3**), we next asked whether mSWI/SNF PLDs can interact with each other and form co-condensates in living cells. To test this, we co-expressed pairs of PLDs with a GFP tag and a mCherry tag. In our first set of studies, we took advantage of the very low C_{sat} of SS18^{PLD}, which forms condensates robustly upon expression in the cell nucleus and used it as the scaffold PLD for live cell experiments. Heterotypic PLD interactions within phase-separated GFP-tagged SS18^{PLD} condensates in live cells were probed by the degree of mCherry-tagged client PLD partitioning. We used mCherry alone as a reference. We observed that SS18^{PLD} condensates recruit other PLDs in cellulo (**Fig. 4a**). Quantification of the degree of partitioning revealed that while ARID1A and ARID1B are strongly enriched within SS18^{PLD} condensates, BRG1^{PLD} only exhibited mildly enhanced enrichment compared to the mCherry control, whereas FUS^{PLD} showed a strong level of colocalization (**Fig. S6**). This observed trend in our cellular assays is consistent with our results from in vitro partitioning experiments performed with purified proteins (**Fig. 3**), further supporting that heterotypic PLD interactions are sequence-specific. We next performed similar experiments with ARID1A^{PLD} (**Fig. S7**) and ARID1B^{PLD} (**Fig. S8**) as scaffold condensates and made similar observations that except for BRG1^{PLD}, other PLDs strongly partition within the scaffold condensates. However, we noted that Pol II CTD[30] did not significantly enrich within condensates of any of the three mSWI/SNF PLDs in cells (**Fig. S9**). This observation contrasts with our in vitro client recruitment assay results showing moderate degrees (k ~ 20−80) of enrichment (**Fig. 3**). This may be due to post-translational modification of the Pol II CTD in cells, specifically, phosphorylation, which was previously shown to inhibit Pol II CTD recruitment to condensates formed by the FET family PLDs [61].

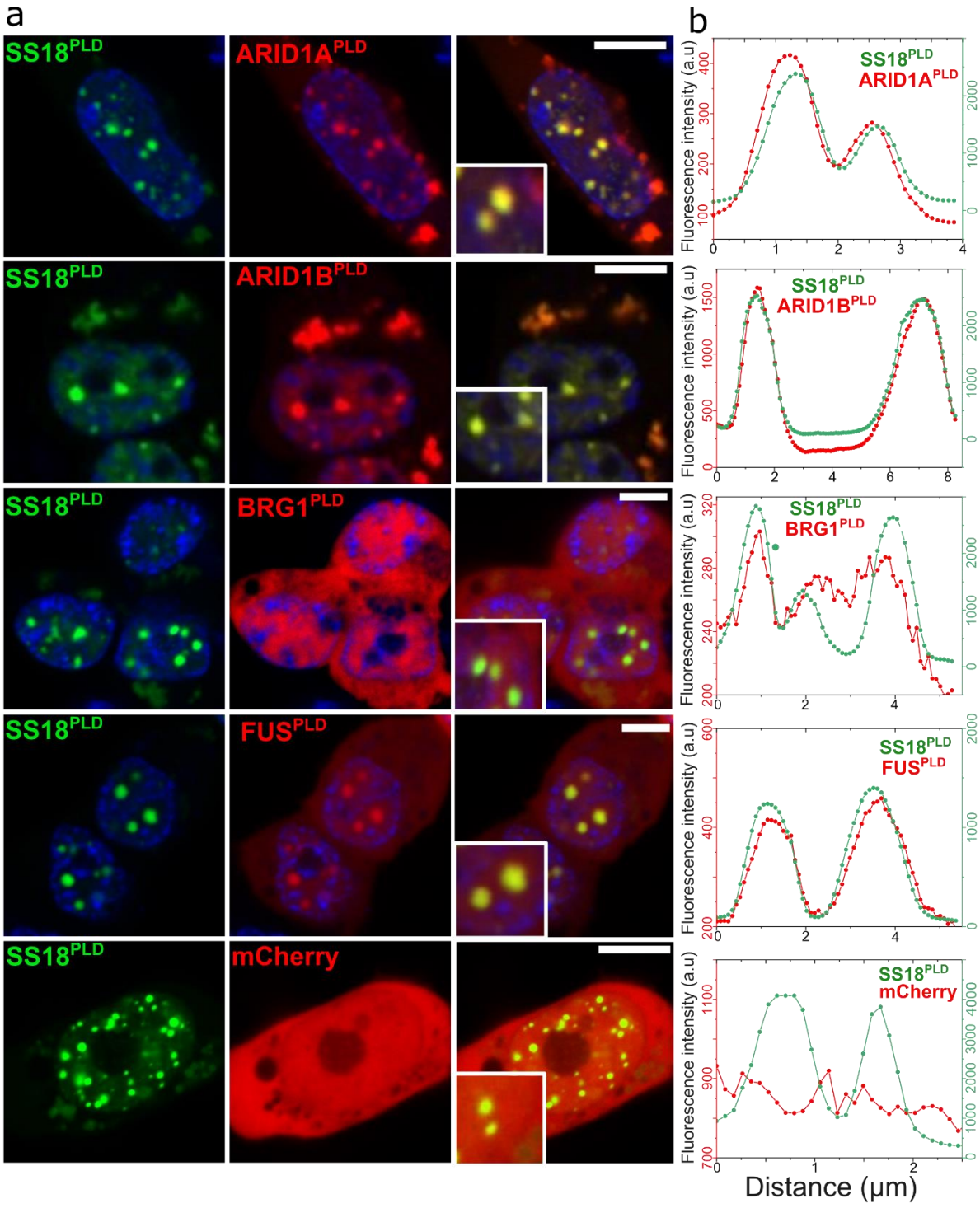

Figure 4: Heterotypic PLDs co-condense in live cells. a) HEK293T cells co-expressing GFP-SS18^{PLD} and either one of the mCherry-tagged PLDs (ARID1A^{PLD}, ARID1B^{PLD}, FUS^{PLD} and BRG1^{PLD}) or mCherry alone. **b)** The degree of colocalization is displayed as intensity profiles for condensates shown in the *inset* images. Green represents the intensity profile of GFP-SS18^{PLD} and red represents the profile for mCherry-tagged PLD. The enrichment coefficients are reported in **Fig. S6**. The scale bar is 10 microns for all images.

mSWI/SNF PLDs lower the saturation concentration of FUS^{PLD} and form spatially homogeneous co-condensates

How do heterotypic PLD interactions impact the phase behavior of multi-component PLD mixtures encompassing FUS and mSWI/SNF subunit PLDs? To systematically address this, we chose FUS^{PLD} as our primary PLD system, which phase separates with a saturation concentration of ~ 200 μM in vitro (**Fig. S2a**), giving us a broad range of concentrations to test. To probe how mSWI/SNF PLDs affect FUS^{PLD} phase separation, we choose two specific PLD systems: ARID1A^{PLD}, which features strong heterotypic interactions with FUS^{PLD}, and BRG1^{PLD} that has weak heterotypic interactions with FUS^{PLD} (**Fig. 3** & **Figs. S6-8**). While FUS^{PLD} (C_{sat} ~ 200 μM) has moderate phase separation driving force, BRG1^{PLD} (C_{sat} > 200 μM) has a substantially lower tendency to undergo phase separation and ARID1A^{PLD} (C_{sat} = 2.5 μM) is highly phase separation competent (**Fig. 1** & **Fig. S2a**). We observed that in the presence of both ARID1A^{PLD} and BRG1^{PLD} at concentrations below their respective C_{sat}, the saturation concentration of FUS^{PLD} is lowered in a non-linear fashion (**Fig. 5a** & **Fig. S10**). These observations suggest that heterotypic interactions are highly cooperative with homotypic interactions in driving phase separation of the PLD mixtures [5]. In the co-PLD phase diagram (**Fig. 5a**), we identify five specific regimes: regimes (I) and (V) are homotypic phase separation regimes of the two PLDs; regime (II) is a single-phase regime where the mixture of PLDs stay soluble; regime (III) is a PLD co-condensation regime where each of the component PLD concentrations is less than their respective C_{sat} but the mixture undergoes phase separation; and regime (IV) is another PLD co-condensation regime where each of the component PLD concentrations is higher than their respective C_{sat}.

Two emergent features of the two-component PLD phase diagrams (**Fig. 5a** & **Fig. S10**) are worth highlighting. The first of them is our observation that the PLD mixtures co-phase separate under conditions where the single PLD component concentrations are below their respective C_{sat} (regime III). In biomolecular mixtures of multiple PLD components, the phase separation driving forces are effectively determined by the synergistic balance of homotypic and heterotypic PLD interactions. Intriguingly, the lowering of C_{sat} of FUS^{PLD} by mSWI/SNF subunit PLDs (**Fig. 5a** & **Fig. S10**) shows a concave trend, which is indicative of positive cooperativity where the heterotypic interactions enhance the phase separation of the mixture [5]. Therefore, in this case, the heterotypic PLD interactions dominate over the homotypic interactions leading to an effective lowering of the C_{sat} of either of the PLD chains.

The second key feature of the ternary PLD mixture is the mixing of PLD dense phases within the co-condensates even though the C_{sat} of individual PLDs differ by almost two orders of magnitude (**Fig. 1** & **Fig. S2**). This is evident from confocal fluorescence microscopy images, which revealed that the ternary PLD mixtures formed co-condensates that are spatially homogeneous in regimes III and IV (**Figs. 5a-c**). The co-mixing of individual PLD phases within ternary PLD condensates (**Fig. 5d**) was not only observed in vitro but also in live cells when two PLDs were co-expressed (**Fig. 3; Figs. S7&S8**). These observations again suggest that the homotypic and heterotypic PLD interactions are either highly similar or the heterotypic interactions are dominant in this system. We reason the latter to be the most plausible case based on our experimentally determined two-component phase diagrams (**Fig. 5a** & **Fig. S10**) and the discussion above. If the homotypic chain interactions were dominant over heterotypic interactions in the ternary mixture, multi-phasic

condensate morphologies may emerge [47,49,62,63] with spatially co-existing individual PLD phases, which is the opposite of our experimental observations (**Fig. 5b-d** & **Fig. S10**).

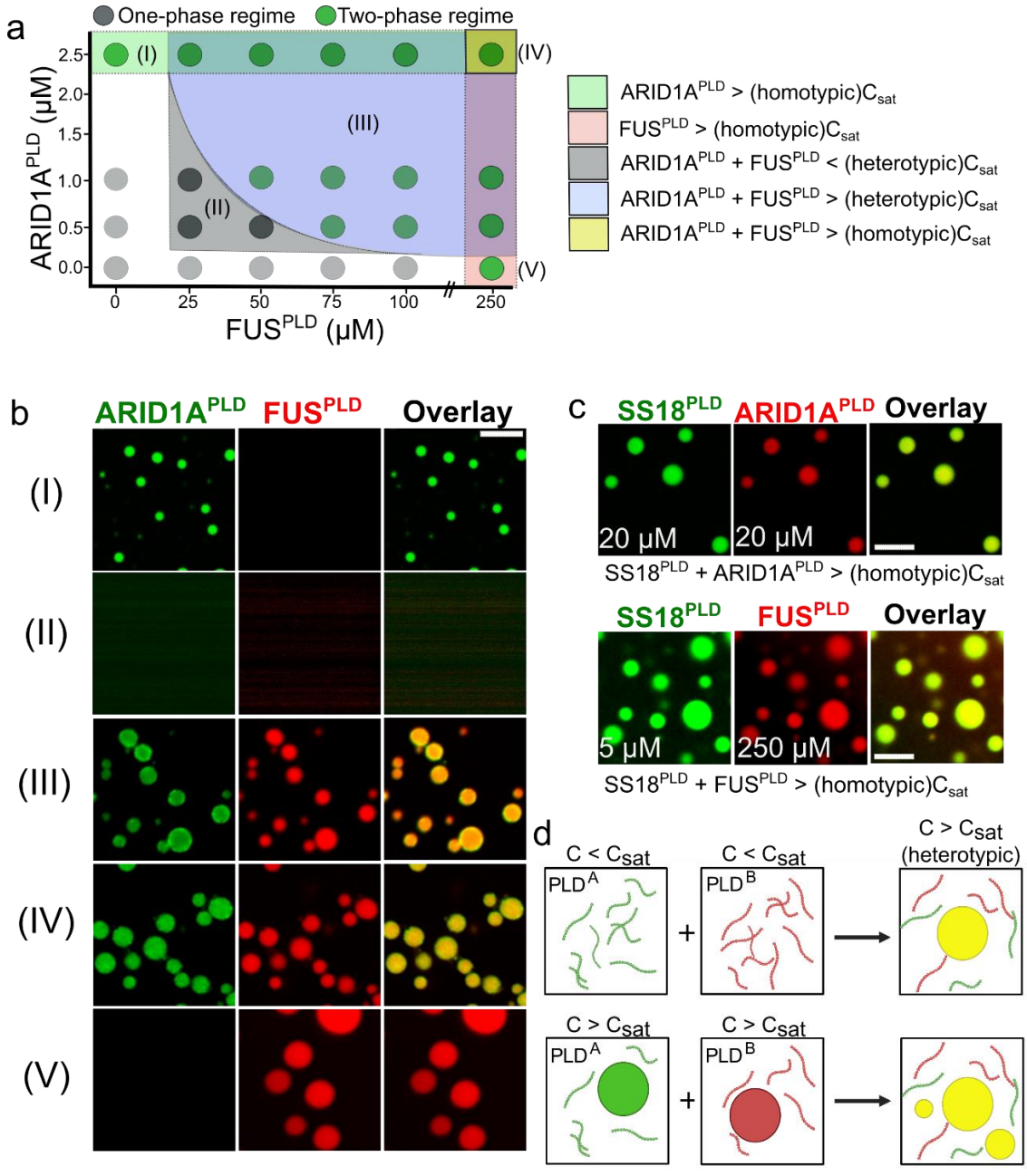

Figure 5: Heterotypic PLD interactions promote phase separation and form monophasic PLD co-condensates. **a)** Co-phase diagram of FUS^{PLD} and $ARID1A^{PLD}$ shows lowering of saturation concentration of heterotypic PLD mixtures. The green circles indicate two-phase regimes, and the grey circles indicate single-phase regimes. The legend provides the description of the shaded regions highlighted in five distinct colors. **b)** Fluorescence microscopy images of PLD samples from the specific regions of the phase diagram shown in (**a**). $ARID1A^{PLD}$ is labeled with AlexaFluor488

and FUS^{PLD} is labeled with AlexaFluor594. **c)** Fluorescence microscopy images of PLD co-condensates formed by the mixtures of SS18^{PLD} with ARID1A^{PLD} (top) and SS18^{PLD} with FUS^{PLD} (bottom) at concentrations above the saturation concentrations of respective PLDs. SS18^{PLD} is labeled with AlexaFluor488, ARID1A^{PLD}, and FUS^{PLD} are labeled with AlexaFluor594, respectively. The scale bar is 5 microns for all images. **d)** A schematic showing formation of monophasic ternary PLD co-condensates, corresponding to regimes III and IV in the phase diagram shown in (**a**). This is created with BioRender.com.

Heterotypic PLDs interact in the sub-saturation concentrations

In our experiments thus far, we observed that condensates formed by mSWI/SNF subunit PLDs can recruit other PLDs in vitro and in live cells. Further, heterotypic PLD interactions lead to a lowering of FUS^{PLD} saturation concentration and the formation of spatially homogeneous PLD co-condensates. Since heterotypic interactions seem to dominate over homotypic interactions in ternary PLD mixtures (**Fig. 5** & **Fig. S10**), we next asked whether these PLDs interact with each other at concentrations below their saturation concentrations. To address this, we first employed a bead halo assay [64] with a pair of PLDs. In these experiments, AlexaFluor488-labeled scaffold PLDs containing a hexahistidine (His_6) tag were immobilized on the surface of Ni-NTA micro-spheres through Ni-His_6 interactions. The scaffold PLD was designed to contain a solubility tag (MBP; see Materials and Methods) to abrogate phase separation on the bead surface. We used two mSWI/SNF PLDs, SS18^{PLD} and BRG1^{PLD}, as scaffolds in our experiments. The scaffold PLD concentration used for these measurements was fixed at 250 nM, which is much lower than their respective C_{sat}. As a negative control, we used a His_6-MBP-GFP that is not expected to interact with the PLD chains. Next, 250 nM of AlexaFluor594-labeled FUS^{PLD} (client PLD) was added to the solution (**Fig. 6a**). We expect that if heterotypic PLD interactions are present at these scaffold-client concentrations that are much lower than their C_{sat}, they would enable recruitment of the client PLD (FUS^{PLD}) to the bead surfaces coated with a scaffold PLD (SS18^{PLD} or BRG1^{PLD}). Further, the relative degree of client recruitment will depend on the strength of scaffold-client interactions, with SS18^{PLD} being a significantly stronger scaffold than the BRG1^{PLD} (**Fig. 3**). Indeed, we observed that FUS^{PLD} is preferentially recruited on the SS18^{PLD}- and BRG1^{PLD}-coated beads as compared to the GFP-coated beads (**Fig. 6b&c**). These data suggest that SS18^{PLD} and BRG1^{PLD} interact with FUS^{PLD} at a concentration much lower than their saturation concentrations. We further noted that the relative FUS^{PLD} enrichment was much higher on SS18^{PLD}-coated beads as compared to BRG1^{PLD}-coated beads (**Fig. 6c**). These results not only provide evidence of the presence of heterotypic PLD-PLD interactions at their sub-saturation concentrations but also lend further support that the heterotypic interactions between FUS^{PLD} and mSWI/SNF component PLDs are sequence-specific (**Fig. 6c**). We further attempted to quantify apparent binding affinities by titrating FUS^{PLD} concentration and keeping the scaffold PLD concentration fixed. However, instead of an apparent two-state binding isotherm, we observed a monotonic increase in the enrichment of FUS^{PLD} on the bead surface (**Fig. S11**) as the FUS^{PLD} concentration increased. This observation may suggest non-stoichiometric binding and homotypic interactions between the FUS^{PLD} on the surface of the bead at higher client concentrations [65,66].

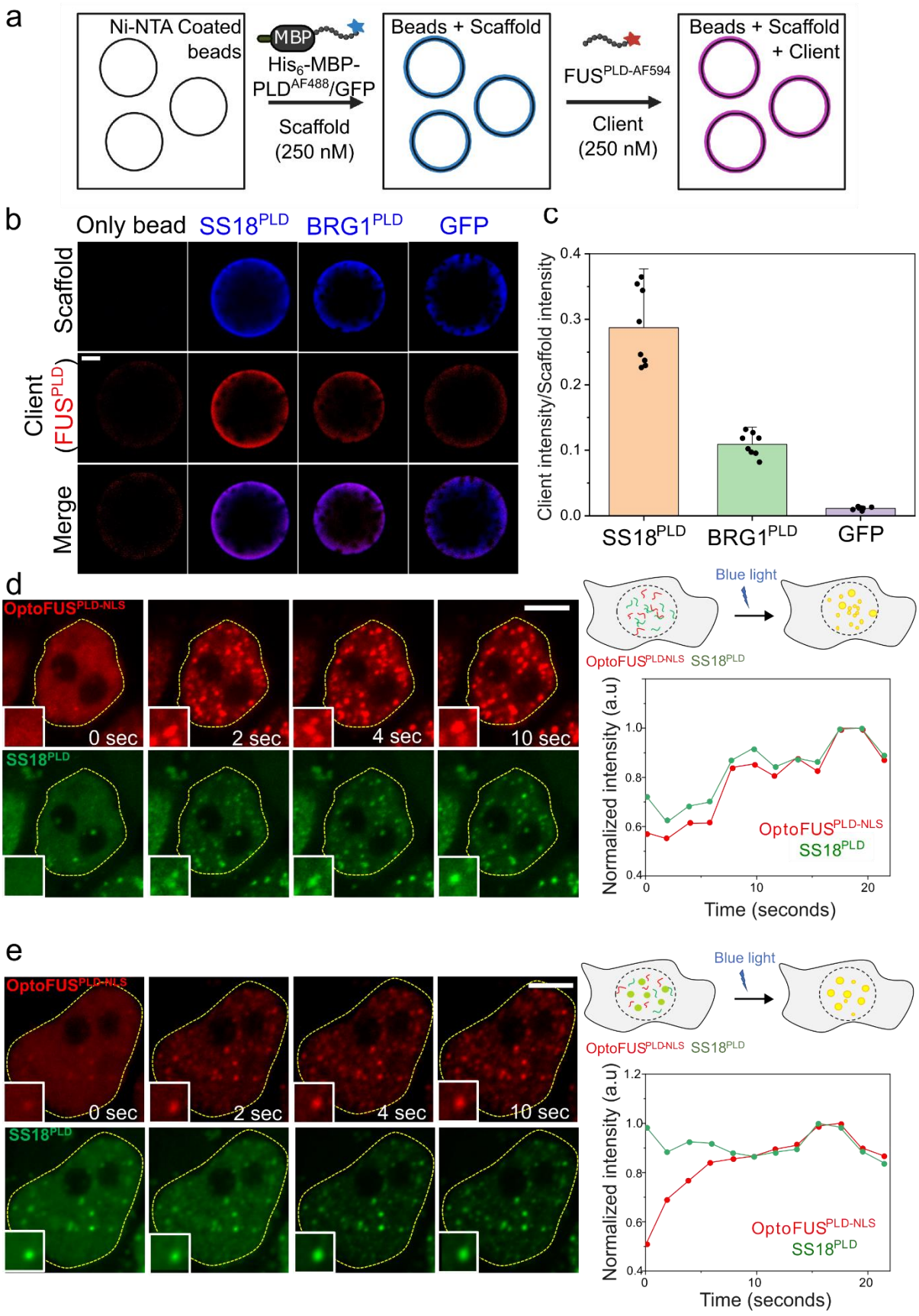

Figure 6: Heterotypic PLDs interact at sub-saturation concentrations. a) A schematic representation of the bead halo assay. Created with BioRender.com. **b)** 250 nM of AlexaFluor488-labeled His_6-MBP-PLD (either $SS18^{PLD}$ or $BRG1^{PLD}$) or control His_6-MBP-GFP was attached to Ni-NTA beads. 250 nM of FUS^{PLD} labeled with AlexaFluor594 was then added to the above beads (see Materials and Methods for further details). Binding was quantified using the ratio of fluorescence intensities (fluorescence signal from FUS^{PLD}/fluorescence signal from the scaffold PLD or GFP control) on the surface of the bead. **c)** A bar chart of the intensity ratios is plotted along with the mean and standard deviation (n = 8 beads). **d)** HEK293T cells co-expressing $OptoFUS^{PLD-NLS}$ (Cry2-mCherry-$FUS^{PLD-NLS}$) and GFP-$SS18^{PLD}$ below their saturation concentrations. Upon blue light activation, $OptoFUS^{PLD}$ co-condenses with GFP-$SS18^{PLD}$. Mean intensity profiles of the co-condensates formed are shown as a function of time for condensates within the inset image. Green represents the intensity profile of GFP-$SS18^{PLD}$ and red represents the intensity profile for $OptoFUS^{PLD}$. The corresponding movie is shown in **Movie S1**. **e)** Pre-existing GFP-$SS18^{PLD}$ clusters act as nucleation sites for $OptoFUS^{PLD}$ condensates upon blue light activation (also see **Movie S2** & **Movie S3)**. The scale bar is 5 microns for all images.

The occurrence of heterogeneous nanoscopic oligomers of FUS in the pre-phase separation regime has recently been reported [38]. Our observations that heterotypic PLDs interact and recruit each other on the bead surface at concentrations several orders of magnitude lower than their saturation concentrations now suggest that heterotypic interactions between prion-like LCDs can also occur in the dilute phase independent of phase separation. However, a key unanswered question is whether such interactions take place in the complex intracellular microenvironment of a living cell. To test heterotypic interactions between mSWI/SNF subunit PLDs and FUS^{PLD} in absence of phase separation, we employed a light-activated phase separation approach [48]. In this assay, we used an $optoFUS^{PLD-NLS}$ construct to induce FUS^{PLD} condensation in live cell nucleus using blue light, while co-expressing GFP-$SS18^{PLD}$ near sub-saturation level (**Fig. 6d**). When FUS^{PLD} condensation was actuated by blue light, we made two key observations. The first one was that $SS18^{PLD}$ was enriched simultaneously at sites where $optoFUS^{PLD-NLS}$ condensates were formed upon blue light activation (**Fig. 6d** & **Movie S1**). We note that in this case, there were no pre-existing $SS18^{PLD}$ condensates. Secondly, we observed that in cells containing pre-existing $SS18^{PLD}$ clusters, they acted as nucleation centers for $optoFUS^{PLD}$ condensation (**Fig. 6e** & **Movie S2**). This feature is further highlighted in cells with multiple pre-existing $SS18^{PLD}$ condensates where $optoFUS^{PLD}$ condensation only occurred at those sites (**Fig. S12** & **Movie S3**). Collectively, we conclude that FUS and SS18 PLDs form soluble complexes in the dilute phase below their saturation concentrations and $SS18^{PLD}$ clusters can nucleate condensation of the FUS^{PLD} in live cells (**Fig. 6d&e; Fig. S12**).

Discussion

mSWI/SNF (also known as BAF) complex is a multi-subunit ATP-dependent chromatin remodeler with critical functions in genome organization and spatiotemporal transcriptional programming during development [42,43,67,68]. Mutations in mSWI/SNF subunits including ARID1A/B, BRG1, and SS18 are linked to multiple tumor types. However, apart from the ATP-dependent catalytic activity of the subunit BRG1 in nucleosome repositioning and eviction [69,70], the functions of other subunits in controlling chromatin landscape are less understood. Interestingly, one common feature among ARID1A/B, BRG1, and SS18 primary sequences is that they all have long stretches (~ 300-500 amino acids) of disordered low-complexity domains without any known functions [44]. Sequence analysis revealed that these LCDs are prion-like (**Fig. S1**) [28]. Employing in vitro experiments with purified LCDs as well as cell culture models, here we show that AIRD1A/B and SS18 PLDs

undergo liquid-liquid phase separation with saturation concentrations substantially lower than previously reported PLDs from RNA binding proteins, including FUS^{PLD} (**Fig. 1** & **Fig. S2**). While aromatic residues have been shown to play a major role in driving PLD phase separation [18,19], here we find that the strong phase separation driving forces for the PLDs of SS18 and ARID1A/B arise from their longer chain length as compared to FUS^{PLD}. We tested this idea by increasing the FUS^{PLD} chain length two-fold, which resulted in a substantially lower intracellular saturation concentration of FUS^{2XPLD}, similar to the PLDs of SS18 and ARID1A/B. However, despite of similar chain length, $BRG1^{PLD}$, which contains significantly reduced numbers of aromatic stickers (**Tables S1-3**), showed a very weak driving force for phase separation (C_{sat} > 200 μM; **Fig. 1** & **Fig. S2**), highlighting that longer chain length alone is not sufficient for driving phase separation of PLDs. Together, these results suggest that PLD chain length along with the number and strength of aromatic stickers collectively governs their phase separation driving force.

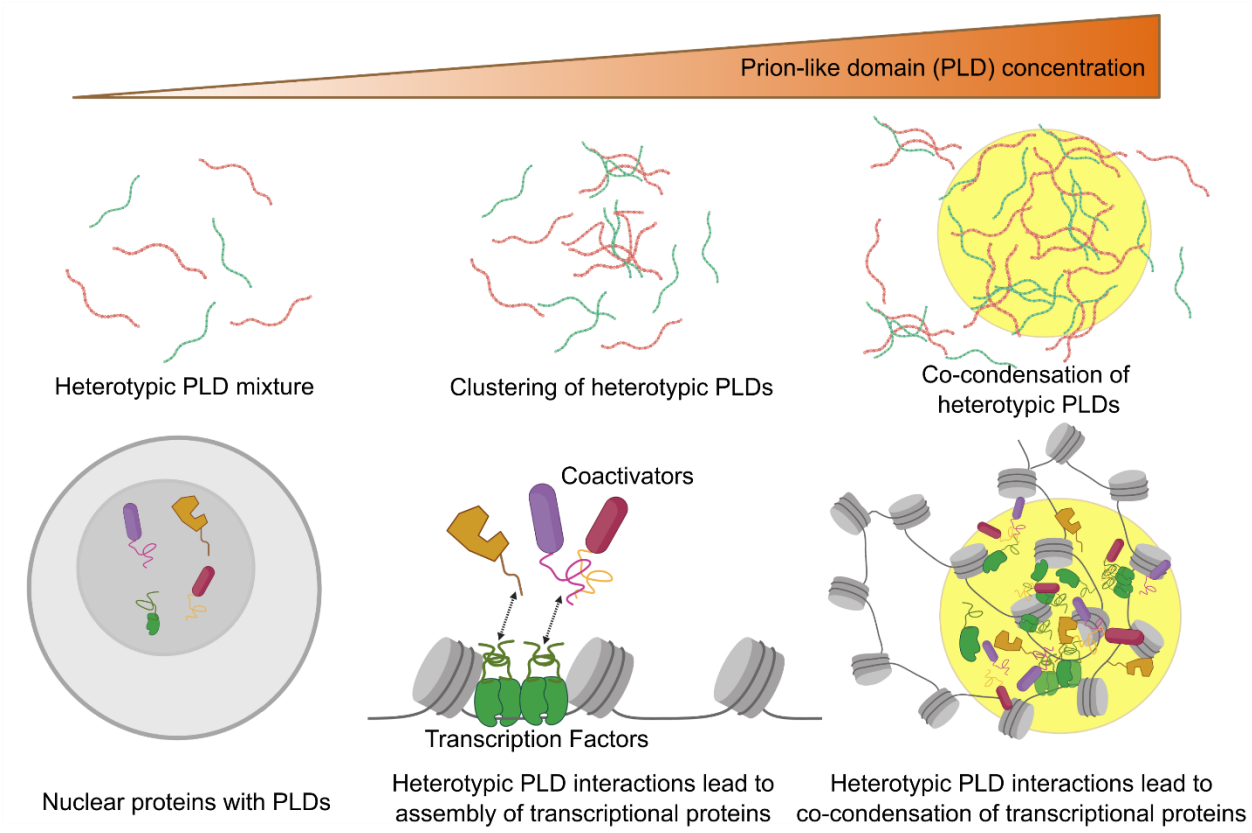

Figure 7: Schematic illustration of heterotypic PLD-mediated co-assemblies driving functional protein interaction networks. Heterotypic PLD interactions occur in the dilute phase at sub-saturation concentrations which upon increasing protein concentration can lead to co-phase separation of the mixture into spatially homogeneous multi-component condensates (top panel). Our results collectively suggest that transcriptional proteins can be assembled into co-phase-separated hubs through sequence-specific positively cooperative interactions among low-complexity domains (bottom panel). Created with BioRender.com.

Although the saturation concentrations of the PLDs of SS18 and ARID1A/B and FUS^{PLD} differ by two orders of magnitude at a fixed temperature (**Fig. 1** & **Fig. S2**), mSWI/SNF subunit PLD condensates formed completely miscible co-condensates with FUS^{PLD} in vitro and in live cells

(**Figs. 4&5**). This observation seems apparently puzzling at first based on the difference in C_{sat} values of respective PLD chains, which may represent highly dissimilar strengths of homotypic inter-chain interactions in FUS^{PLD} and mSWI/SNF PLDs. If the homotypic interactions are substantially different in a ternary mixture of polymers, it can form coexisting dense phases with differential densities [47,62,63]. However, as shown in (**Fig. 2)** and discussed above, the difference in the C_{sat} values between the mSWI/SNF PLDs and FUS^{PLD} likely stems from the difference in their chain length, with mSWI/SNF PLDs having much longer chains. According to the polymer model, the free energy of liquid-liquid phase separation is an inverse function of the chain length [71]. Therefore, the lower saturation concentration of mSWI/SNF PLDs likely arises from their increased chain length, where longer chains act as an entropic sink, rather than stronger interactions between the chains [72]. Further, our ternary phase diagrams (**Fig. 5** & **Fig. S10**) suggest that heterotypic interactions between these PLD chains are dominant over the homotypic interactions in PLD mixtures, which is also consistent with the observed miscibility of FUS^{PLD} condensates with ARID1A^{PLD} and SS18^{PLD} condensates. Such positive cooperativity in interactions between PLDs of mSWI/SNF subunits and that of FET proteins may have important functional relevance in the formation of transcriptional hubs where transcription factors and coactivators can coexist in a single homogeneous phase-separated hub.

Prion-like LCDs provide unique properties to a protein such as the ability to self-associate and the capability to engage with heterotypic PLDs [28,34,37]. It is therefore not surprising that PLDs are enriched in proteins that play a role within the same biological process such as transcription initiation, where multivalent heterotypic PLD interactions can allow transcription factors and co-activators to assemble through co-phase separation (**Fig. 7**). Our results on the mixtures of PLDs reducing the saturation concentration for phase separation of the individual components suggest that transcription factors and co-activators can enhance phase separation of each other through co-scaffolding (**Fig. 7**). This implies that multiple proteins with PLDs can provide a positive cooperative effect to reduce the concentration required for phase separation of the collection of proteins. We speculate that heterotypic PLD-mediated positive cooperativity in protein-protein interactions is likely to play key roles in the assembly and operation of SWI/SNF complexes and their interactions with transcription factors containing similar low-complexity domains [28,35,36,73].

The ability of the FET family of transcription factors containing an N-terminal PLD to orchestrate oncogenic gene expression has recently been linked to their aberrant interactions with the BAF complex subunits, such as BRG1[36,40]. Given multiple mSWI/SNF subunits contain long PLDs, could such interactions be mediated by these intrinsically disordered LCDs (**Fig. 7**)? Indeed, our results suggest that mSWI/SNF subunit PLDs can engage in sequence-specific interactions with each other and with the PLD of FUS. Previously, heterotypic interactions have been reported for transcription factors containing PLDs such as EBF1 and FUS [35]. We further tested this idea by co-expressing FUS and a fusion oncoprotein FUS-DDIT3 containing an N-terminal PLD in the same cells. We observed that FUS strongly co-localizes within FUS-DDIT3 condensates (**Fig. S13**). Since PLDs are common in many endogenous and cancer-associated fusion transcription factors, based on our results reported here, we propose a common mode of functional protein-protein interactions in transcriptional regulation for these factors through sequence-specific heterotypic interactions between low-complexity protein domains.

Finally, a key finding of our study is that the PLD-mediated multivalent interactions can occur at sub-micromolar concentrations below their saturation concentrations (**Figs. 6&7**). These results imply that heterotypic PLD-mediated protein-protein interactions are likely to be present at physiologically relevant protein concentrations inside living cells. Such interactions can lead to the formation of heterotypic clusters at the single-phase regime, similar to homotypic pre-percolation clusters observed for RNA-binding proteins [38]. Given intracellular concentrations of many proteins at their endogenous level often resides at sub-saturation level [74], our results reported in this work suggest that the functional protein-protein networks can arise from heterotypic interactions mediated by multivalent LCDs in the dilute phase independent of phase separation.

Acknowledgments

This work was supported by the US National Institute of General Medical Sciences (NIGMS) of the National Institutes of Health grant award (R35 GM138186) to P.R.B. The initial part of this work was supported by the US National Institute on Aging (NIA) of the National Institutes of Health grant award (R21 AG064258) to P.R.B. The authors gratefully acknowledge the members of the Banerjee Lab, Dr. Rohit Pappu and Dr. Tanja Mittag for valuable feedback during the course of manuscript preparation.

Author contributions

Conceptualization: P.R.B. and R.B.D.; Methodology: P.R.B., R.B.D., and A.K.R.; Investigation: P.R.B., R.B.D., M.M.M., and A.K.R.; Resources: P.R.B.; Writing – original draft: P.R.B., M.M.M., and R.B.D.; Writing – reviewing and editing: all authors; Funding acquisition: P.R.B.

Competing interests

All authors declare no competing interests.

References

1. Banani, S. F., Lee, H. O., Hyman, A. A. & Rosen, M. K. Biomolecular condensates: organizers of cellular biochemistry. *Nat. Rev. Mol. Cell Biol.* **18**, 285–298 (2017).
2. Sabari, B. R., Dall'Agnese, A. & Young, R. A. Biomolecular Condensates in the Nucleus. *Trends Biochem. Sci.* **45**, 961–977 (2020).
3. Alberti, S. & Hyman, A. A. Biomolecular condensates at the nexus of cellular stress, protein aggregation disease and ageing. *Nat. Rev. Mol. Cell Biol.* **22**, 196–213 (2021).
4. March, Z. M., King, O. D. & Shorter, J. Prion-like domains as epigenetic regulators, scaffolds for subcellular organization, and drivers of neurodegenerative disease. *Brain Res.* **1647**, 9–18 (2016).
5. Farag, M., Borcherds, W. M., Bremer, A., Mittag, T. & Pappu, R. V. Phase Separation in Mixtures of Prion-Like Low Complexity Domains is Driven by the Interplay of Homotypic

and Heterotypic Interactions. *bioRxiv* 2023.03.15.532828 (2023) doi:10.1101/2023.03.15.532828.

6. Lancaster, A. K., Nutter-Upham, A., Lindquist, S. & King, O. D. PLAAC: a web and command-line application to identify proteins with prion-like amino acid composition. *Bioinformatics* **30**, 2501–2502 (2014).
7. Alberti, S., Halfmann, R., King, O., Kapila, A. & Lindquist, S. A systematic survey identifies prions and illuminates sequence features of prionogenic proteins. *Cell* **137**, 146–158 (2009).
8. Tetz, G. & Tetz, V. Prion-like Domains in Eukaryotic Viruses. *Sci. Rep.* **8**, 8931 (2018).
9. Espinosa Angarica, V., Ventura, S. & Sancho, J. Discovering putative prion sequences in complete proteomes using probabilistic representations of Q/N-rich domains. *BMC Genomics* **14**, 316 (2013).
10. Zajkowski, T. *et al.* The Hunt for Ancient Prions: Archaeal Prion-Like Domains Form Amyloid-Based Epigenetic Elements. *Molecular Biology and Evolution* **38**, 2088–2103 (2021).
11. Garai, S. *et al.* Plant Prionome maps reveal specific roles of prion-like proteins in stress and memory. *bioRxiv* 2020.09.25.311993 (2020).
12. Tetz, G. & Tetz, V. Prion-Like Domains in Phagobiota. *Frontiers in Microbiology* **8**, 2239 (2017).
13. Murakami, T. *et al.* ALS/FTD Mutation-Induced Phase Transition of FUS Liquid Droplets and Reversible Hydrogels into Irreversible Hydrogels Impairs RNP Granule Function. *Neuron* **88**, 678–690 (2015).
14. King, O. D., Gitler, A. D. & Shorter, J. The tip of the iceberg: RNA-binding proteins with prion-like domains in neurodegenerative disease. *Brain Res.* **1462**, 61–80 (2012).
15. Jaunmuktane, Z. & Brandner, S. Invited Review: The role of prion-like mechanisms in neurodegenerative diseases. *Neuropathol. Appl. Neurobiol.* **46**, 522–545 (2020).
16. Fowler, D. M., Koulov, A. V., Balch, W. E. & Kelly, J. W. Functional amyloid--from bacteria to humans. *Trends Biochem. Sci.* **32**, 217–224 (2007).
17. Franzmann, T. M. & Alberti, S. Prion-like low-complexity sequences: Key regulators of protein solubility and phase behavior. *J. Biol. Chem.* **294**, 7128–7136 (2019).
18. Martin, E. W. *et al.* Valence and patterning of aromatic residues determine the phase behavior of prion-like domains. *Science* **367**, 694–699 (2020).
19. Bremer, A. *et al.* Deciphering how naturally occurring sequence features impact the phase behaviours of disordered prion-like domains. *Nat. Chem.* **14**, 196–207 (2022).
20. Molliex, A. *et al.* Phase separation by low complexity domains promotes stress granule assembly and drives pathological fibrillization. *Cell* **163**, 123–133 (2015).
21. Gotor, N. L. *et al.* RNA-binding and prion domains: the Yin and Yang of phase separation. *Nucleic Acids Res.* **48**, 9491–9504 (2020).
22. Boncella, A. E. *et al.* Composition-based prediction and rational manipulation of prion-like domain recruitment to stress granules. *Proc. Natl. Acad. Sci. U. S. A.* **117**, 5826–5835 (2020).
23. Choi, K.-J. *et al.* NANOG prion-like assembly mediates DNA bridging to facilitate chromatin reorganization and activation of pluripotency. *Nat. Cell Biol.* (2022) doi:10.1038/s41556-022-00896-x.
24. Davis, R. B., Moosa, M. M. & Banerjee, P. R. Ectopic biomolecular phase transitions: fusion proteins in cancer pathologies. *Trends Cell Biol.* **32**, 681–695 (2022).
25. Schwartz, J. C., Cech, T. R. & Parker, R. R. Biochemical Properties and Biological Functions of FET Proteins. *Annu. Rev. Biochem.* **84**, 355–379 (2015).
26. Lin, Y., Currie, S. L. & Rosen, M. K. Intrinsically disordered sequences enable modulation of protein phase separation through distributed tyrosine motifs. *J. Biol. Chem.* **292**, 19110–19120 (2017).

27. Wang, J. *et al.* A Molecular Grammar Governing the Driving Forces for Phase Separation of Prion-like RNA Binding Proteins. *Cell* **174**, 688-699.e16 (2018).
28. Davis, R. B., Kaur, T., Moosa, M. M. & Banerjee, P. R. FUS oncofusion protein condensates recruit mSWI/SNF chromatin remodeler via heterotypic interactions between prion-like domains. *Protein Sci.* **30**, 1454–1466 (2021).
29. Owen, I. *et al.* The oncogenic transcription factor FUS-CHOP can undergo nuclear liquid-liquid phase separation. *bioRxiv* 2021.02.24.432743 (2021) doi:10.1101/2021.02.24.432743.
30. Patel, A. *et al.* A Liquid-to-Solid Phase Transition of the ALS Protein FUS Accelerated by Disease Mutation. *Cell* **162**, 1066–1077 (2015).
31. Zhang, Y.-J. *et al.* The dual functions of the extreme N-terminus of TDP-43 in regulating its biological activity and inclusion formation. *Hum. Mol. Genet.* **22**, 3112–3122 (2013).
32. Fomicheva, A. & Ross, E. D. From Prions to Stress Granules: Defining the Compositional Features of Prion-Like Domains That Promote Different Types of Assemblies. *Int. J. Mol. Sci.* **22**, (2021).
33. Harrison, A. F. & Shorter, J. RNA-binding proteins with prion-like domains in health and disease. *Biochem. J.* **474**, 1417–1438 (2017).
34. Frazer, C. *et al.* Epigenetic cell fate in Candida albicans is controlled by transcription factor condensates acting at super-enhancer-like elements. *Nature Microbiology* **5**, 1374–1389 (2020).
35. Wang, Y. *et al.* A Prion-like Domain in Transcription Factor EBF1 Promotes Phase Separation and Enables B Cell Programming of Progenitor Chromatin. *Immunity* **53**, 1151-1167.e6 (2020).
36. Boulay, G. *et al.* Cancer-Specific Retargeting of BAF Complexes by a Prion-like Domain. *Cell* **171**, 163-178.e19 (2017).
37. Huang, X. *et al.* Heterotypic transcriptional condensates formed by prion-like paralogous proteins canalize flowering transition in tomato. *Genome Biol.* **23**, 78 (2022).
38. Kar, M. *et al.* Phase-separating RNA-binding proteins form heterogeneous distributions of clusters in subsaturated solutions. *Proc. Natl. Acad. Sci. U. S. A.* **119**, e2202222119 (2022).
39. Deniz, A. A. Percolation physics and density transition frameworks converge in biomolecular condensation. *Proc. Natl. Acad. Sci. U. S. A.* **119**, e2210177119 (2022).
40. Lindén, M. *et al.* FET family fusion oncoproteins target the SWI/SNF chromatin remodeling complex. *EMBO Rep.* **20**, e45766 (2019).
41. Mittal, P. & Roberts, C. W. M. The SWI/SNF complex in cancer - biology, biomarkers and therapy. *Nat. Rev. Clin. Oncol.* **17**, 435–448 (2020).
42. Centore, R. C., Sandoval, G. J., Soares, L. M. M., Kadoch, C. & Chan, H. M. Mammalian SWI/SNF Chromatin Remodeling Complexes: Emerging Mechanisms and Therapeutic Strategies. *Trends Genet.* **36**, 936–950 (2020).
43. Kadoch, C. & Crabtree, G. R. Mammalian SWI/SNF chromatin remodeling complexes and cancer: Mechanistic insights gained from human genomics. *Sci. Adv.* **1**, e1500447 (2015).
44. El Hadidy, N. & Uversky, V. N. Intrinsic Disorder of the BAF Complex: Roles in Chromatin Remodeling and Disease Development. *Int. J. Mol. Sci.* **20**, (2019).
45. Thway, K. & Fisher, C. Synovial sarcoma: defining features and diagnostic evolution. *Ann. Diagn. Pathol.* **18**, 369–380 (2014).
46. Mittag, T. & Pappu, R. V. A conceptual framework for understanding phase separation and addressing open questions and challenges. *Mol. Cell* **82**, 2201–2214 (2022).
47. Kaur, T. *et al.* Sequence-encoded and composition-dependent protein-RNA interactions control multiphasic condensate morphologies. *Nat. Commun.* **12**, 872 (2021).
48. Shin, Y. *et al.* Spatiotemporal Control of Intracellular Phase Transitions Using Light-Activated optoDroplets. *Cell* vol. 168 159-171.e14 (2017).

49. Welles, R. M. *et al.* Determinants of disordered protein co-assembly into discrete condensed phases. *bioRxivorg* (2023) doi:10.1101/2023.03.10.532134.
50. Burke, K. A., Janke, A. M., Rhine, C. L. & Fawzi, N. L. Residue-by-residue view of in vitro FUS granules that bind the C-terminal domain of RNA polymerase II. *Mol. Cell* **60**, 231–241 (2015).
51. Maharana, S. *et al.* RNA buffers the phase separation behavior of prion-like RNA binding proteins. *Science* **360**, 918–921 (2018).
52. Hofweber, M. & Dormann, D. Friend or foe-Post-translational modifications as regulators of phase separation and RNP granule dynamics. *J. Biol. Chem.* **294**, 7137–7150 (2019).
53. Guilak, F., Tedrow, J. R. & Burgkart, R. Viscoelastic properties of the cell nucleus. *Biochem. Biophys. Res. Commun.* **269**, 781–786 (2000).
54. Rosowski, K. A. *et al.* Elastic ripening and inhibition of liquid-liquid phase separation. *Nat. Phys.* **16**, 422–425 (2020).
55. Zhang, Y., Lee, D. S., Meir, Y., Brangwynne, C. P. & Wingreen, N. S. Mechanical frustration of phase separation in the cell nucleus by chromatin. *Biophys. J.* **122**, 6a (2023).
56. Varga, J., Kube, M., Luck, K. & Schick, S. The BAF chromatin remodeling complexes: structure, function, and synthetic lethalities. *Biochem. Soc. Trans.* **49**, 1489–1503 (2021).
57. Bracha, D. *et al.* Mapping Local and Global Liquid Phase Behavior in Living Cells Using Photo-Oligomerizable Seeds. *Cell* **175**, 1467-1480.e13 (2018).
58. Zhou, M. *et al.* Phase-separated condensate-aided enrichment of biomolecular interactions for high-throughput drug screening in test tubes. *J. Biol. Chem.* **295**, 11420–11434 (2020).
59. Banani, S. F. *et al.* Compositional Control of Phase-Separated Cellular Bodies. *Cell* **166**, 651–663 (2016).
60. Pei, G., Zhou, M., Xu, W., Wang, J. & Li, P. Phase Separation-Based Biochemical Assays for Biomolecular Interactions. *Methods Mol. Biol.* **2563**, 225–236 (2023).
61. Wei, M.-T. *et al.* Nucleated transcriptional condensates amplify gene expression. *Nat. Cell Biol.* **22**, 1187–1196 (2020).
62. Lu, T. & Spruijt, E. Multiphase Complex Coacervate Droplets. *J. Am. Chem. Soc.* **142**, 2905–2914 (2020).
63. Feric, M. *et al.* Coexisting liquid phases underlie nucleolar subcompartments. *Cell* **165**, 1686–1697 (2016).
64. Patel, S. S. & Rexach, M. F. Discovering novel interactions at the nuclear pore complex using bead halo: a rapid method for detecting molecular interactions of high and low affinity at equilibrium. *Mol. Cell. Proteomics* **7**, 121–131 (2008).
65. Tompa, P. & Fuxreiter, M. Fuzzy complexes: polymorphism and structural disorder in protein-protein interactions. *Trends Biochem. Sci.* **33**, 2–8 (2008).
66. Mitrea, D. M. *et al.* Self-interaction of NPM1 modulates multiple mechanisms of liquid–liquid phase separation. *Nat. Commun.* **9**, 842 (2018).
67. Ho, P. J., Lloyd, S. M. & Bao, X. Unwinding chromatin at the right places: how BAF is targeted to specific genomic locations during development. *Development* **146**, (2019).
68. Hodges, C., Kirkland, J. G. & Crabtree, G. R. The Many Roles of BAF (mSWI/SNF) and PBAF Complexes in Cancer. *Cold Spring Harb. Perspect. Med.* **6**, (2016).
69. Khavari, P. A., Peterson, C. L., Tamkun, J. W., Mendel, D. B. & Crabtree, G. R. BRG1 contains a conserved domain of the SWI2/SNF2 family necessary for normal mitotic growth and transcription. *Nature* **366**, 170–174 (1993).
70. Wang, W. *et al.* Purification and biochemical heterogeneity of the mammalian SWI-SNF complex. *EMBO J.* **15**, 5370–5382 (1996).
71. Rubinstein, M. & Colby, R. H. Polymer physics. http://boulderschool.yale.edu/sites/default/files/files/Polymer_Physics_Lectures2&3_Rubinstein.pdf (2003).

72. Liu, C. *et al.* Phase Separation in Multicomponent Aqueous-Protein Solutions. *J. Phys. Chem.* **99**, 454–461 (1995).
73. Brahma, S. & Henikoff, S. RNA Polymerase II, the BAF remodeler and transcription factors synergize to evict nucleosomes. *bioRxivorg* (2023) doi:10.1101/2023.01.22.525083.
74. Erdel, F. & Rippe, K. Formation of Chromatin Subcompartments by Phase Separation. *Biophys. J.* **114**, 2262–2270 (2018).